

# Four-fermion simulation at LEP2 in DELPHI

A. Ballestrero<sup>1,2</sup> \*, R. Chierici<sup>1</sup>, F. Cossutti<sup>3</sup> and E. Migliore<sup>2,4</sup>

<sup>1</sup> CERN, CH-1211 Geneva, Switzerland.

<sup>2</sup> INFN, Sezione di Torino, IT-10125 Torino, Italy.

<sup>3</sup> INFN, Sezione di Trieste, IT-34127 Trieste, Italy.

<sup>4</sup> Dipartimento di Fisica Sperimentale, Università di Torino, IT-10125 Torino, Italy.

## Abstract

We present and discuss the generator setup for  $e^+e^- \rightarrow 4f$  processes chosen by the DELPHI collaboration. The need to combine the most recent theoretical achievements in the CC03 sector with the state of the art description of the remaining part of the 4-fermion processes has led to an original combination of different codes, with the WPHACT 2.0 4-fermion generator and the YFSWW code for the CC03  $\mathcal{O}(\alpha)$  corrections as a starting point. The coverage of the 4-fermion phase space is discussed in detail, with particular attention to ensuring the compatibility of WPHACT with dedicated  $\gamma\gamma$  generators.

# 1 Introduction

This report presents the description of the generator setup which has been developed for the simulation of four-fermion ( $4-f$ ) processes at LEP, and used by the DELPHI experiment for the final LEP2 analyses.

A large variety of first order Feynman diagrams contribute to the production of four fermions in  $e^+e^-$  interactions, depending on the specific final state. The possible processes are divided into 3 classes: charged current (CC), neutral current (NC), and mixed current (MIX), the last receiving contributions from both charged and neutral current diagrams. The detailed classification of the  $4-f$  final states used throughout this paper is the one usually adopted at LEP2 [1], and can be found for instance in [2]. All the  $4-f$  final states described in this classification are listed in appendix B. The different families of Feynman diagrams contributing to the production of  $4-f$  final states at tree level are presented in [3]; they are conventionally classified as either  $t$ -channel or  $s$ -channel diagrams, the former referring to diagrams with at least one boson propagator in the  $t$ -channel. Thus  $t$ -channel diagrams are always present for processes with at least one electron (or positron) in the final state.

The origin of the work described in this paper is in the outcome of the 2000 LEP2 Monte Carlo workshop [4] and subsequent work by the theory community. They have addressed the problems posed by the LEP experiments in the 4-fermion sector, which were basically: 1) to provide a theoretical precision in the description of the  $WW$  physics significantly better than the anticipated experimental one; 2) to supply good modelling of the remaining 4-fermion processes, in order to compare with the LEP measurements and to give a solid description of the background to the new physics signals searched for at LEP.

The most important request for  $WW$  physics concerned the use of  $\mathcal{O}(\alpha)$  radiative corrections in the so-called Double Pole Approximation (DPA) [5,6]. For the virtual part these corrections are applied only to CC03 diagrams, – those which correspond to production and decay of the two  $W$ s. At present, two Monte Carlo codes include the DPA corrections: RacoonWW [7], which makes use of the results of ref. [6], and YFSWW [8], which implements the electroweak corrections to  $WW$  production of reference [9] and the Khoze-Chapovsky ansatz [10] for the non-factorizable corrections. Different strategies are also used for real part corrections. For a detailed analysis of the two approaches and their numerical consistency we refer to [4].

It has been demonstrated that the more complete inclusion of first order corrections leads to significant effects in the precision measurements at LEP2 [11]. In particular, their effects on differential distributions are so important that the inclusion of those computations in the physics generators at LEP2 is essential. In addition, there are several other features that are very desirable (or necessary) to have in a  $4-f$  generator when studying non-CC03 processes as a signal, or when considering them as a background to new physics searches. They range from a fully massive calculation over all the phase space to efficient integration in singular regions, the inclusion of higher order corrections, etc, and they have been either unavailable or only partially available in the past.

From the experimentalist's point of view, the ideal  $4-f$  generator which includes all the above-mentioned features did not exist to our knowledge at the end of the LEP2 Monte Carlo workshop; in general, generators which were best suited for CC03 physics did not include the desirable  $4-f$  features, and vice-versa. This posed a serious problem of matching between the treatment of different phase space regions in a coherent event generation.

It is important to note that the  $4-f$  processes overlap with the so-called  $\gamma\gamma$  ones. The overlap is entire for the leptonic  $eell$  final state,<sup>1</sup> and for the direct photon component (i.e. when the photon behaves as a point-like particle) in the hadronic  $eeqq$  final state. In the phase space region where the  $\gamma\gamma$  processes dominate, dedicated codes are usually preferred to  $4-f$  generators both because they contain the description of the resolved photon component for the  $eeqq$  final state and because they provide a more efficient generation. The matching of the genuine  $4-f$  part to the  $\gamma\gamma$  dominated one therefore has to be done carefully in order to allow a complete and smooth coverage of the whole experimentally accessible phase space.

## 2 The DELPHI approach

The DELPHI approach consists in interfacing two generators to keep as many features as possible for both CC03 and non-CC03 physics. There are two ways of doing this:

- **Independent generation:** This consists of two independent event generations, one for the CC03 part with  $\mathcal{O}(\alpha)$  DPA corrections and one for the remaining amplitudes. The  $4-f$  matrix element squared in DPA approximation,  $|4f|_{DPA}^2$ , can be decomposed in the following way:

$$|4f|_{DPA}^2 = |4f|^2 - |\text{CC03}|^2 + |\text{CC03}_{DPA}|^2 = |4f - \text{CC03}|^2 + \text{Int.} + |\text{CC03}_{DPA}|^2, \quad (1)$$

where  $4f$  is the 4-fermion matrix element without DPA corrections, while CC03 and  $\text{CC03}_{DPA}$  represent the CC03 part without and with their inclusion. In our notation  $\text{Int.}$  is the interference term between the CC03 part and the rest. It is relevant to note that this term is computed by using CC03 as given by the Improved Born Approximation (IBA). With an independent generation one can either neglect this term, thus introducing a systematic effect of particular importance for processes of the CC20 class which involve electrons in the final states, or it is possible to include the interference in the pure  $4-f$  part. In the latter case, however, it is possible that the event weight defined in this way, i.e.  $|4f - \text{CC03}|^2 + \text{Int.}$ , becomes negative in certain regions of the phase space.

- **Reweighting:** This basically consists in generating the whole  $4-f$  phase space with only one generator, then reweighting events to account for the DPA corrections. This correction is intended to affect only the CC03 part. The weights are defined as ratios of matrix elements squared, as we will describe in the following.

We have chosen to adopt the second approach, since dedicated studies have shown that the negative weight problem in the first one can become quite sizeable, affecting, for instance, as many as 20% of the events in the  $qqe\nu$  final states, and is therefore difficult to treat when an unweighted event generation is needed.

The **KandY** concurrent generators combination [12] has shown that the second approach provides an effective, though approximate, solution to the problem, implemented by reweighting full  $4-f$  events (in the original approach generated with **KORALW** [13]) with the matrix element provided by the **YFSWW** [8] calculation, in which the  $\mathcal{O}(\alpha)$  radiative corrections are calculated in the leading pole approximation. The structure of the other currently available DPA Monte Carlo calculation, **RacoonWW** [7], with an explicit  $4f + \gamma$  massless matrix element, is technically not suitable for such an approach.

<sup>1</sup>Here and elsewhere where the meaning is clear we suppress symbols distinguishing fermion from antifermion in the definition of  $4-f$  states.

We have chosen `WPHACT 2.0` [14] as general 4- $f$  generator on top of which the `YFSWW` reweighting has been implemented. It includes practically all the required features discussed in the introduction:

- fully massive matrix elements and phase space for all the 4- $f$  final states;
- dedicated phase space mappings for the low mass region, with the inclusion of  $q\bar{q}$  resonance production via the package described in [15], and for the small scattering angle region, thus allowing a reliable integration for both these regions where the cross-section is divergent in the massless approximation;
- use of the `QEDPS` [16] library to generate ISR photons with finite transverse momentum, implemented with the  $t$  scale for  $t$ -channel dominated processes;
- Fermion Loop corrections in the IFL (Imaginary part) scheme for single  $W$  processes [17];
- running of  $\alpha_{QED}$ ;
- multiple versions of the Coulomb correction for `CC03` events, including the Khoze-Chapovsky (K-C) screened Coulomb ansatz [10], needed for  $\mathcal{O}(\alpha)$  corrections;
- off-diagonal CKM matrix elements, except  $V_{ub}$ .

In addition, `WPHACT` allows the generation of unweighted events for any user-specified subset of 4- $f$  final states in a single run and the computation of matrix elements with predefined subsets of Feynman diagrams.

In the `DELPHI` customized version several features have been added, which will be described in the next paragraphs:

- the reweighting for the DPA corrections via `YFSWW` has been implemented by interfacing the two codes; in order to allow this the YFS exponentiated treatment of the ISR in leading logarithm approximation at  $\mathcal{O}(\alpha^3)$  used in `YFSWW` and `KORALW` has been ported and interfaced to `WPHACT`;
- the existing interface with the `PYTHIA` [18] hadronization library has been extended to include interfaces with the radiation, hadronization and decay libraries `PHOTOS` [19], `TAUOLA` [20], `ARIADNE` [21], `HERWIG` [22] and the low mass hadronization package [15];
- the possibility to compute the matrix element with different subsets of Feynman diagrams has been used to produce for each event a list of precomputed squared matrix elements at generation level for different contributions to be used in reweightings.

The coverage of the phase space in terms of generation cuts has been studied and optimized with the aim of extending it as much as possible according to the needs of the physics analyses, but keeping under control the numerical accuracy of the phase space integration and of the matrix element calculations. An important part of this work has been the clear definition of the matching with dedicated  $\gamma\gamma$  generators, i.e. of the separation between classes of events to be generated with the 4- $f$  code and those to be generated with specific  $\gamma\gamma$  calculations.

### 3 $\mathcal{O}(\alpha)$ DPA radiative corrections via `YFSWW` reweighting

The weight to be used to account for DPA in 4- $f$  events can be evaluated as a ratio of matrix elements. Using the notation of equation (1) the event weight is written as:

$$w = \frac{|4f|_{DPA}^2}{|4f|^2} = \frac{|4f|^2 - |\text{CC03}|^2 + |\text{CC03}_{DPA}|^2}{|4f|^2} = 1 - \frac{|\text{CC03}|^2}{|4f|^2} \left( 1 - \frac{|\text{CC03}_{DPA}|^2}{|\text{CC03}|^2} \right). \quad (2)$$

In this reweighting procedure the interference term is included, although computed using CC03 as given by the IBA. The numerator in relation (2) can be rewritten in a more concise form as:

$$|4f|_{DPA}^2 = |\text{CC03}|^2(1 + \delta_{4f} + \delta_{DPA}), \quad (3)$$

where:

$$\delta_{4f} = \frac{|4f|^2}{|\text{CC03}|^2} - 1, \quad \delta_{DPA} = \frac{|\text{CC03}_{DPA}|^2}{|\text{CC03}|^2} - 1. \quad (4)$$

This represents the so-called additive approach to the DPA reweighting. In this formulation the new 4- $f$  matrix element results from the CC03 one with the addition of two corrections, one accounting for the presence of extra diagrams due to the 4- $f$  background and the other for the radiative corrections. The advantage of using the additive approach is that it depends only upon two ratios, namely  $|\text{CC03}|^2/|4f|^2$  and  $|\text{CC03}_{DPA}|^2/|\text{CC03}|^2$ . The first term can be calculated event by event with an IBA 4- $f$  generator, while the second can be determined from the output of YFSWW. The YFSWW generator, used as a reweighter, returns the value  $|\text{CC03}_{DPA}|^2/|\text{CC03}_{K-C}|^2$ , i.e. the DPA matrix element with respect to the CC03 one which already includes the Coulomb screening via the Khoze-Chapovsky correction, an effective treatment of the non-factorizable part of the  $\mathcal{O}(\alpha)$  correction. The desired ratio can be determined by multiplying this output by  $|\text{CC03}_{K-C}|^2/|\text{CC03}|^2$ , which gives a very small smearing to the weight distribution, of the order of a per cent.

The reader should bear in mind that the DPA correction can be considered by definition to be reliable only within a few  $\Gamma_W$  around the double resonant pole.

Figure 1 shows the distributions of these matrix element ratios for events with a  $WW$  double resonant (i.e. CC03) contribution generated with WPHACT and reweighted with YFSWW. In plot a) the DPA weight is shown relative to the CC03 weight with the Khoze-Chapovsky screened Coulomb ansatz. The effect of this ansatz is shown in plot b). The lower figures, c) and d), show the derived DPA weight to 4- $f$  as defined in equation (2); the average value of the distribution gives the total cross-section reduction induced by DPA. The small enhancement at  $w_{DPA} = 1$  represents the contribution of the events dominated by the non-CC03 part for which  $|\text{CC03}|^2/|4f|^2 \approx 0$ , essentially CC20 events in the single  $W$  region or mixed events where the neutral current component is dominant.

From plot c) of figure 1, based on the above definition of  $|4f|_{DPA}^2$ , it is evident that there are rare events for which the total DPA weight is negative. These have been investigated and found to be events compatible with CC03 kinematics, with a sizeable and negative interference between the CC03 and non-CC03 diagrams (for the CC20 class they are about 0.1% of the total), and whose CC03 part is very much suppressed by DPA. Thus, from expression (2) it is clear that the global weight can become negative, since the DPA reweighting does not affect the interference term. The solution we have adopted to this problem is to replace the *Int.* term with  $\text{Int.} \times \sqrt{|\text{CC03}_{DPA}|^2/|\text{CC03}|^2}$ . This corrects only the modulus of the interference term and not its phase and it removes in practice the negative weights. The effect of this correction is shown in plot d).

While in YFSWW the radiation from the  $W$ s is also generated, this is not present in normal 4- $f$  generators like KORALW or WPHACT. Thus the reweighting cannot account for this effect, but it considers only the ISR part of the radiation. However, the YFSWW group has shown in [12] that the reweighting procedure of 4- $f$  KORALW events in the additive scheme correctly reproduces the main differential distributions of CC03 events obtained with YFSWW alone, since at LEP2 energies the effect of radiation off  $W$ s is marginal. The robustness of the approach is thus confirmed.

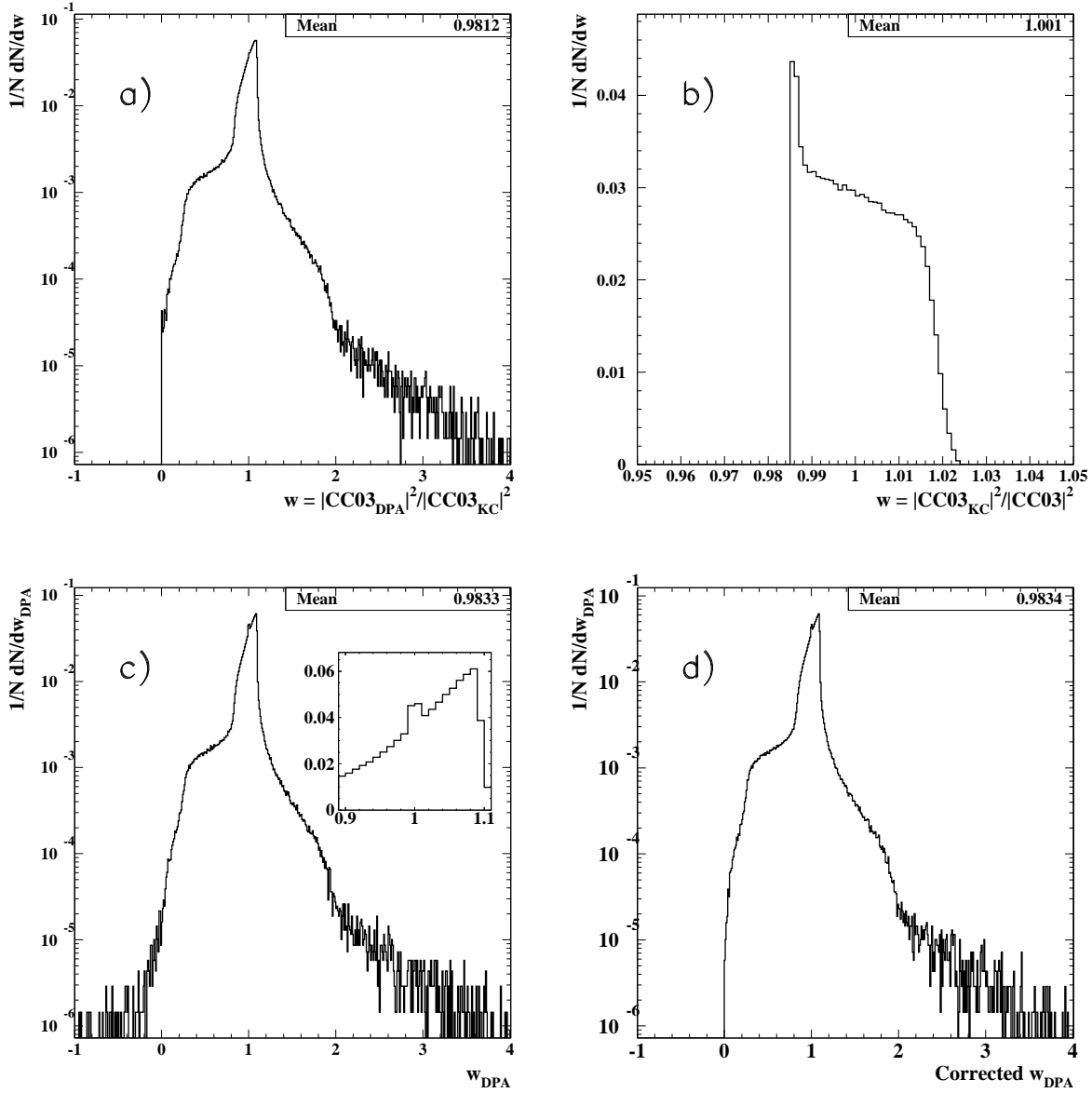


Figure 1: Distribution of weights  $w$  derived from a 4- $f$  sample of events with a  $WW$  double resonant contribution generated with WPHACT at  $\sqrt{s} = 189$  GeV. a): Relative weight of the DPA squared matrix element to the CC03 one with K-C correction applied; b): Relative weight of the CC03 squared matrix element with and without K-C correction; c): the global DPA weight; Inset: the region around the enhancement at 1, due to the non-CC03 contribution; d): the global DPA weight after correction to eliminate negative weights. See text for details of the evaluation of the weights shown.

## 4 Initial state radiation issues

In relation (2) the CC03 matrix element is evaluated as given by the IBA, and therefore already accounts for part of the radiation. In the ratio  $|CC03|^2/|4f|^2$ , the standard ISR factorizes and, therefore, once the value of  $s'$  (the effective squared centre-of-mass energy of the event with the ISR photons removed) is fixed for the event, it is not crucial which radiator function is used for the generation of the detailed kinematics of the photons. But when the DPA reweighting is applied, it is better to use the same function in order to get the same  $\mathcal{O}(\alpha)$  results as implemented in the YFSWW calculation, since it is based on corrections applied to a specific radiator.

For this reason the YFS exponentiation for the ISR in the 4- $f$  generation is used in the phase space regions where the DPA correction has to be applied. This is achieved by interfacing its implementation in KORALW with the WPHACT 4- $f$  generator. The interface was technically possible thanks to the modularity of the calculation using the leading logarithm approximation; this allowed the ISR generation to be isolated from the remaining parts of the code. The YFS radiator is used only for  $s$ -channel dominated processes, whereas QEDPS is maintained for the  $t$ -channel dominated ones, exploiting in this way the dedicated treatment of the ISR for these channels in the original WPHACT code, where the  $t$  scale (defined by the square of the lowest  $t$ -channel  $\gamma$  momentum transfer), is used in this case.

Extensive tests have shown that the interface of KORALW's YFS exponentiated ISR in WPHACT is consistent with the original one in KORALW and YFSWW, both for the total cross-section and differential distributions. This agreement has also been possible thanks to very good matching of results between these codes at Born level for CC03 processes. Table 1 compares the total cross-sections obtained by WPHACT with YFS and YFSWW in different configurations for the process  $u\bar{d}\mu\bar{\nu}$  at  $\sqrt{s} = 189$  GeV. Figures 2 and 3 show the comparison of the two generators on the basic ISR photonic distributions, and figure 4 shows the comparison of the DPA weight  $\frac{|CC03_{DPA}|^2}{|CC03|^2}$  when computed with the original YFSWW standalone code and with the WPHACT/YFSWW tandem.

|           | $\sigma(\text{WPHACT})$ (pb) | $\sigma(\text{YFSWW})$ (pb) | $\sigma(\text{WPHACT})/\sigma(\text{YFSWW})$ |
|-----------|------------------------------|-----------------------------|--|
| IBA no CC | 0.59416(7)                   | 0.59412(7)                  | 1.0001(2)                                    |
| IBA KC-CS | 0.60817(7)                   | 0.60730(7)                  | 1.0014(2)                                    |
| DPA       | 0.59701(8)                   | 0.59650(8)                  | 1.0008(2)                                    |

Table 1: Total cross-sections for the process  $u\bar{d}\mu\bar{\nu}$  at  $\sqrt{s} = 189$  GeV with WPHACT with YFS exponentiation, with YFSWW, and their ratio. The results for simple IBA, IBA with Coulomb corrections in the Khoze-Chapovsky ansatz and in DPA are presented. The error from the integration is shown in parenthesis.

## 5 Final state issues: radiation, hadronization, decays

The standard WPHACT 2.0 generator provides an interface to the PYTHIA hadronization library via a routine which is based on the original PY4FRM PYTHIA interface for 4- $f$  generators. Moreover, it always fills the standard HEPEVT event history common block [23].

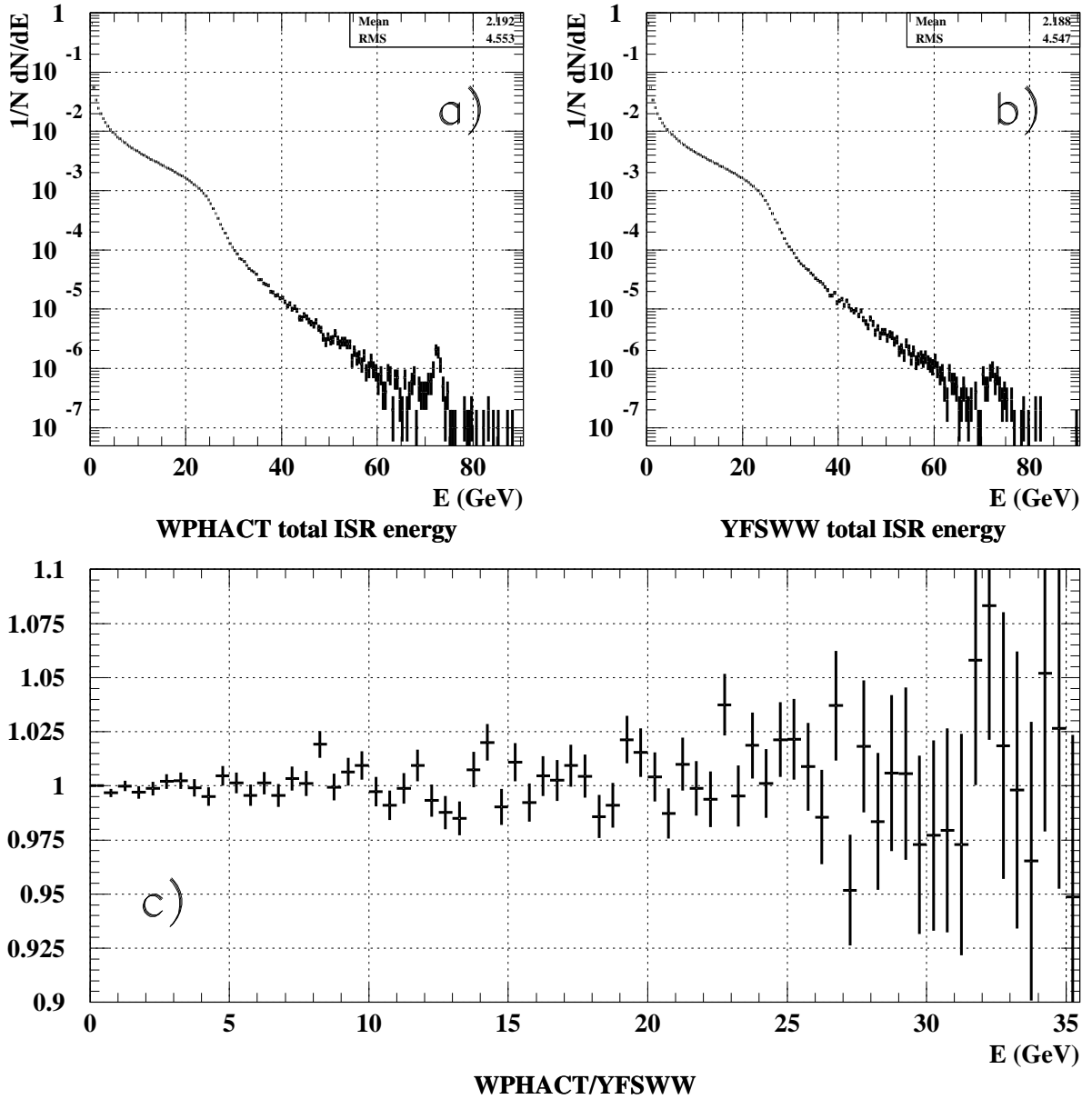


Figure 2: Total ISR photon energy spectrum at Born + ISR level for the process  $u\bar{d}\mu\bar{\nu}$  evaluated at  $\sqrt{s} = 189$  GeV with WPHACT with YFS exponentiation (a) and with YFSWW (b). The difference in their mean values is  $\Delta(\langle E_{ISR} \rangle) = 4 \pm 2$  MeV, where the error is statistical. Plot c) shows the ratio of the two spectra.



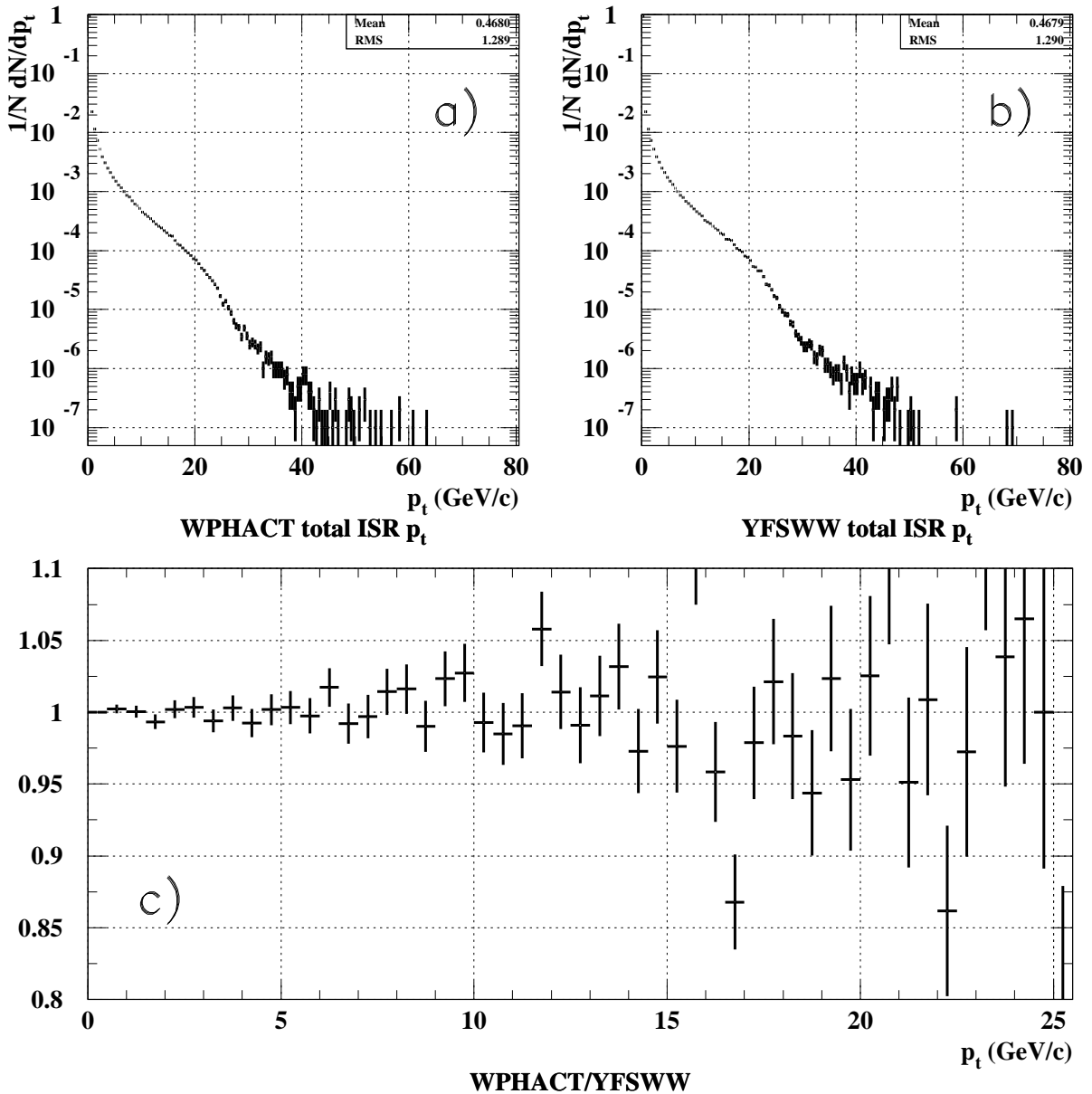


Figure 3: Total photon transverse momentum spectrum at Born + ISR level for the process  $u\bar{d}\mu\bar{\nu}$  evaluated at  $\sqrt{s} = 189$  GeV with WPHACT with YFS exponentiation (a) and with YFSWW (b). The difference in mean values is below the statistical uncertainty of 0.6 MeV. Plot c) shows the ratio of the two spectra.

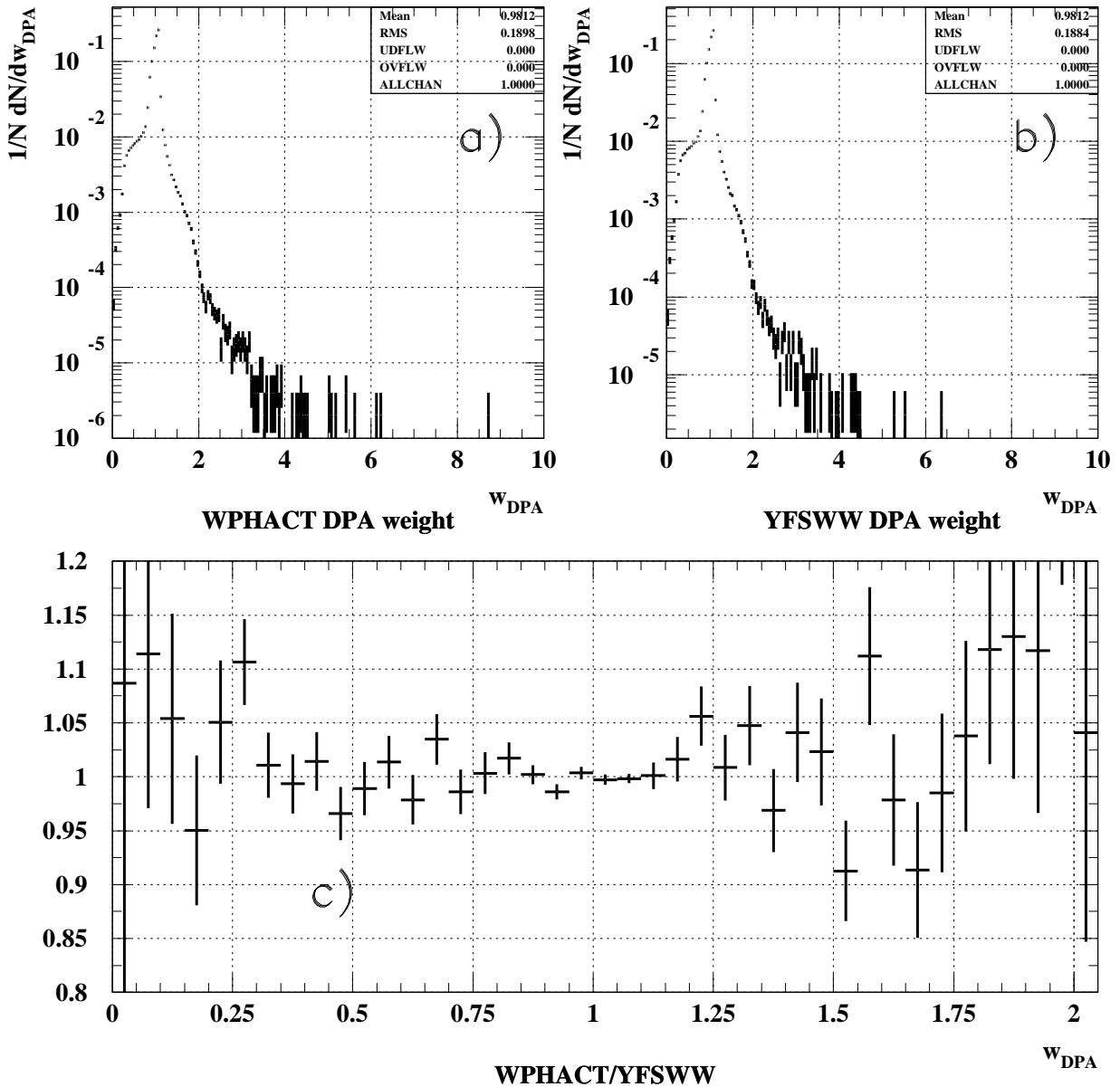


Figure 4: DPA weight  $\frac{|CC03_{DPA}|^2}{|CC03|^2}$  distribution for the process  $u\bar{d}\mu\bar{\nu}$  evaluated at  $\sqrt{s} = 189$  GeV with WPHACT with YFS exponentiation (a) and with YFSWW (b). The two distributions are both normalized to unity. The ratio is shown in plot c).

The event is transformed to the DELPHI reference frame (the incoming electron beam goes in the positive  $z$  axis direction). The interface has then been extended in several ways.

## 5.1 QED final state radiation

The QED final state radiation from leptons is treated as in KORALW/YFSWW. When dealing with charged leptons, the PHOTOS library is called, allowing the production of photons according to a  $\mathcal{O}(\alpha^2)$  leading log calculation. QED radiation from quarks is treated in the hadronization phase by the corresponding libraries. For leptonic  $\gamma\gamma$ -dominated final states the QED final state radiation is switched off in WPHACT, since it is not appropriate to give a realistic description of the data in this region.

## 5.2 $\tau$ decay

The  $\tau$  decays are described with the TAUOLA package, which includes QED radiative corrections for leptonic decays. In the DELPHI interface the  $\tau$  polarization, which is not provided by WPHACT, is defined according to the event topology. The mother boson of each  $\tau$  is identified: if it is a  $W$ , the polarization is defined by the  $\tau$  charge; alternatively, if there is a  $\tau$  pair coming from a  $Z/\gamma^*$ , opposite polarizations are assigned randomly to the taus. TAUOLA is used both for primary taus coming from the hard  $4-f$  process and for those produced in the hadronization cascade.

## 5.3 Quark hadronization

The default hadronization description is given by PYTHIA 6.156 tuned by DELPHI to describe the LEP data at the  $Z$  peak [24]. This version contains the improvements which emerged from the LEP2 generator workshop concerning mass effects in the parton shower and the gluon splitting rate.

Alternatively, the DELPHI tuned versions of ARIADNE 4.08 and HERWIG 6.2 have also been interfaced, the former using the AR4FRM interface provided in the library, the latter with a code based on a former example given by the authors of HERWIG and described in [23]. The availability of different fragmentation models on top of the same electroweak calculation is an essential feature when studying systematic effects. The interface allows comparison of the different colour reconnection and Bose-Einstein correlation schemes implemented in the above hadronization libraries, – a topic of great importance for  $WW$  physics.

A problem to be solved when interfacing the  $4-f$  generator with a hadronization library is the definition of the quark masses. In the electroweak calculation, at least away from the  $\gamma\gamma$ -dominated region, the current algebra masses for the light quarks are the most suited, allowing a realistic description of the  $\gamma^* \rightarrow q\bar{q}$  decay down to 2 pion masses. The heavy quark masses affect the output of the hadronization process, and their values are chosen in order to get the correct gluon splitting rate.

In the hadronization phase the definition has to be consistent with that used in the electroweak calculation, at least from a kinematic point of view. In PYTHIA 6.156 (and ARIADNE, which is essentially a different treatment of the gluon radiation part inserted in PYTHIA) the constituent masses for light quarks are provided as default, but this is not a customary choice for  $e^+e^-$  collider physics, and can be modified. The following set of

masses has therefore been defined to be used both in the electroweak calculations and in the hadronization phase:

$$\begin{aligned}
m(u) &= 0.005 \text{ GeV}/c^2 \\
m(d) &= 0.010 \text{ GeV}/c^2 \\
m(s) &= 0.200 \text{ GeV}/c^2 \\
m(c) &= 1.300 \text{ GeV}/c^2 \\
m(b) &= 4.800 \text{ GeV}/c^2.
\end{aligned}$$

On the other hand, in **HERWIG** the constituent masses for the light quarks are used, and since the mass values are tightly linked to the cluster hadronization model itself, the tuning also depends on them. In order to avoid inconsistencies in the electroweak part while using different hadronization models, the above quark masses have been used in **WPHACT**, and in the interface with **HERWIG** they are modified into the **HERWIG** ones by imposing 4-momentum conservation pair by pair according to the colour connection: in this way the invariant masses of the underlying bosons are preserved, while in general the quark directions are not.

In order to give a consistent picture of the hadronization throughout all the processes, the DELPHI tuned **PYTHIA 6.156** with the above choice of masses has also been used in the 2- $f$  sector (with the **KK2f** [25] generator) and in the Higgs sector (with the **HZHA** [26] generator).

As mentioned before, the above choice is used in all the phase space regions not dominated by multiperipheral diagrams. In the latter case the constituent masses allow a better description of reality, acting as an effective cut-off on the cross-section. Therefore the following values are used for the light quark masses:

$$\begin{aligned}
m(u) &= 0.3 \text{ GeV}/c^2 \\
m(d) &= 0.3 \text{ GeV}/c^2 \\
m(s) &= 0.5 \text{ GeV}/c^2.
\end{aligned}$$

The colour connection scheme used in the presence of mixed charged current and neutral current 4-quark final states exploits the separate generation of the charged and neutral currents in **WPHACT** in such a way as to generate the correct proportion of events of each kind, including the interference between the two: in this way it is known *a priori* whether the current event has to be hadronized, for instance, as  $u\bar{d}d\bar{u}$  (i.e.  $WW$ ) or as  $u\bar{u}d\bar{d}$  (i.e.  $ZZ$ ).

The only ambiguous case is in the presence of 4 identical quarks  $q_1\bar{q}_1q_2\bar{q}_2$  ( $q_1 = q_2$ ), where the approach adopted is as discussed in [23] and also used in **PYTHIA**: the quark pairing is randomly chosen according to the relative probability of each of the two configurations as given by the ratio of the squared amplitudes  $|\mathcal{M}(q_1\bar{q}_1 + q_2\bar{q}_2)|^2/|\mathcal{M}(tot)|^2$  and  $|\mathcal{M}(q_1\bar{q}_2 + q_2\bar{q}_1)|^2/|\mathcal{M}(tot)|^2$ . The event pairing choice is recorded in the standard output of the generator.

## 5.4 Low $q\bar{q}$ mass system hadronization

The string model is not suitable to describe the hadronization of  $q\bar{q}$  systems below a mass of 2 GeV/c<sup>2</sup>. The package in [15] provides a description of the hadronization from the  $\gamma^* \rightarrow q\bar{q}$  process in this low mass region both due to the presence of hadronic

resonances (with subsequent decays described by PYTHIA) and in the continuum, based on experimental  $e^+e^-$  data at low energy. The package has been fully interfaced with WPHACT and, when the quark pairing algorithm described above gives rise to a  $q\bar{q}$  pair of mass below  $2 \text{ GeV}/c^2$ , it is used instead of the other hadronization models to produce the final hadronic state.

## 6 Phase space cuts and matching with $\gamma\gamma$ generators

Ideally the 4- $f$  generation should cover the whole experimentally accessible phase space without any cut. In practice a compromise has to be found between the needs of the physics analyses and the numerical and physical reliability of the calculation, both in terms of matrix element evaluation and of phase space integration. Although the use of FORTRAN quadruple precision arithmetic can significantly boost the numerical stability in delicate regions of the phase space (very low electron angles and very low  $\gamma^*$  masses), it is more CPU consuming and not available in all compilers. In any case, one does not want to produce a huge fraction of generally uninteresting events.

A dedicated study has therefore been performed to define a set of cuts which can realize the above compromise. The basic set of cuts on fermion-antifermion invariant masses and fermion (and antifermion) energies applied to all the final states is shown in table 2.

| Phase space cuts   |
|--|
| Fermion-antifermion invariant mass   |
| $m(q_i\bar{q}_i) > \max(2 m_\pi, 2 m_{q_i})$<br>$m(q_i\bar{q}_j) > \max(2 \text{ GeV}/c^2, m_{q_i} + m_{q_j})$<br>$m(e^+e^-) > 0.2 \text{ GeV}/c^2$  |
| Fermion energy   |
| $E(q) > 1 \text{ GeV}$<br>$E(e) > 1 \text{ GeV}$ if $5^\circ < \theta_e < 175^\circ$<br>$E(\mu) > 1 \text{ GeV}$ if $2^\circ < \theta_\mu < 178^\circ$<br>$E(\tau) > 1 \text{ GeV}$ if $2^\circ < \theta_\tau < 178^\circ$ |

Table 2: Phase space cuts common to all processes.  $q$  means quark,  $e$ ,  $\mu$  and  $\tau$  the charged leptons.  $\theta$  is the polar angle of the fermion. Implicit invariant mass cuts given by the fermion masses are not listed.

In some classes of events additional requirements have been imposed:

CC18 ( $e\nu\mu\nu, e\nu\tau\nu$ ):  $5^\circ < \theta_e < 175^\circ$  or  $5^\circ < \theta_{\mu,\tau} < 175^\circ$ , i.e. there must be at least one visible lepton;

MIX56 ( $e\nu e\nu$ ):  $5^\circ < \theta_{e^-} < 175^\circ$  or  $5^\circ < \theta_{e^+} < 175^\circ$ .

As explained in the previous paragraphs, particular care is needed when treating the NC48 ( $eeqq, ee\mu\mu, ee\tau\tau$ ) and NC144 ( $eeee$ ) final states, which get contributions from the multiperipheral diagrams, and in particular by the direct photon component of the  $\gamma\gamma$  process.

In the description of the  $eeqq$  final state, most general 4- $f$  generators correctly compute the unresolved photon part of the  $\gamma\gamma$  interaction, dominant at high photon virtualities,

where the photon is treated as a pointlike particle. However, they usually cannot properly handle the resolved photon part, i.e. the part where the hadronic content of the photon becomes relevant, and is described by partonic distributions or by the vector meson dominance ansatz, depending on the virtuality range. Dedicated codes model the process in a more realistic way in the phase space region where the resolved photon component starts to be important; usually the non- $\gamma\gamma$  related Feynman diagrams are neglected, since in this region they are highly suppressed. In DELPHI, this part of the phase space has been treated using `PYTHIA 6.143`. The pure direct photon part, corresponding to the multiperipheral diagrams with two photons exchanged in the  $t$ -channel, and the diagram involving at least one resolved photon are added incoherently. This splitting allows use of the full  $4-f$  calculation for the former in the phase space regions where the non-multiperipheral contribution is still relevant, preserving at the same time `PYTHIA`'s description of the latter everywhere.

Three different regions of the phase space have been identified for  $eeff$  final states:

- the “ $4-f$  like” region, where the multiperipheral contribution is not dominant and `WPHACT` with the current algebra masses for the light quarks can be considered fully reliable;
- the “ $\gamma\gamma$  like” region, where the multiperipheral contribution starts to be the dominant one but other electroweak contributions are important and need to be properly described; in this region `WPHACT` with constituent masses for light quarks is used, as discussed above, and the QED final state radiation from leptons generated with `PHOTOS` is switched off;
- the pure  $\gamma\gamma$  region, described with the dedicated codes. For the fully leptonic final states, `BDKRC` [27] has been used for the  $ee\mu\mu$  and  $ee\tau\tau$  final states, since it contains the matrix element with  $\mathcal{O}(\alpha)$  radiative corrections. For the  $eeee$  final state the dedicated code `BDK` [28] is used, mainly for reasons of technical reliability.

The detailed description of the phase space cuts defining these three regions is given in appendix A.

Figure 5 shows, for events belonging to all the  $\gamma\gamma$  compatible final states (i.e.  $eeqq$  and  $eell$ ) at  $\sqrt{s} = 189$  GeV, the fractions of the total squared event matrix element in the “ $\gamma\gamma$  like” region corresponding to different subsets of Feynman diagrams. It can be seen (figure 5a) that the  $t$ -channel component is largely dominant, as expected. The multiperipheral diagrams constitute a large fraction of the total (figure 5b) – almost half of the events’ matrix elements are almost identical to the purely multiperipheral ones; – furthermore those corresponding to genuine direct photon  $\gamma\gamma$  diagrams are clearly the dominant part of the multiperipherals (figure 5c). But it can also be seen that there is a sizeable component where the non-multiperipheral  $t$ -channel diagrams dominate (figure 5d), and the interference between these and all the rest is not negligible in about half of the events (figure 5e). Since the  $s$ -channel hardly contributes in this region, this interference is essentially between the multiperipheral and non-multiperipheral  $t$ -channel amplitudes.

One must be aware that the cuts used in the “ $\gamma\gamma$  like” region still leave some numerical instability of the order of a few per cent when using double precision. This is found comparing, for instance, `WPHACT` double and quadruple precision results for  $eeu\bar{u}$  single tag events with  $10^\circ < \theta_e < 170^\circ$  and  $3 < m(u\bar{u}) < 40$  GeV/ $c^2$  (see appendix A) at various energies. Normally the difference is of the order of 2%, but values as high as 6% have been found. This difference diminishes and rapidly disappears if the lower value of  $m(u\bar{u})$  is increased by a few GeV/ $c^2$ . The above numerical instability is in any case well below

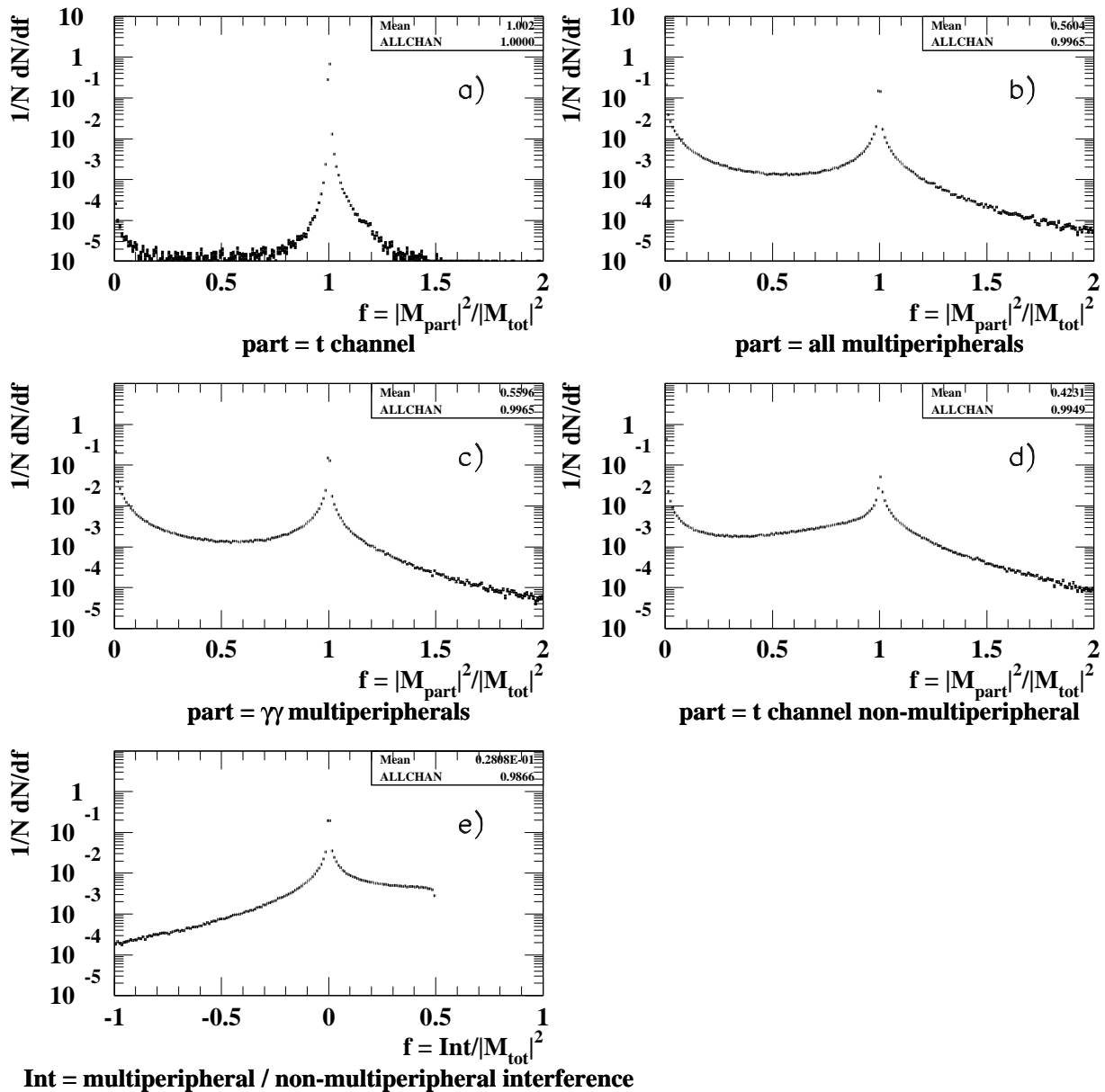


Figure 5: a)–d): Spectra of the fractions  $f = |\mathcal{M}_{part}|^2 / |\mathcal{M}_{tot}|^2$  of the total squared event matrix element  $|\mathcal{M}_{tot}|^2$  corresponding to different subsets of Feynman diagrams (labelled as *part*) for events belonging to all the  $\gamma\gamma$  compatible final states (i.e.  $eeqq$  and  $eell$ ) in the “ $\gamma\gamma$  like” region at  $\sqrt{s} = 189$  GeV: a)  $t$ -channel diagrams, b) multiperipheral diagrams, c) multiperipheral diagrams with only photon exchange (i.e. direct photon  $\gamma\gamma$ ), d)  $t$ -channel non-multiperipheral diagrams; e) interference between the multiperipheral part and the remaining amplitude.

the estimated theoretical uncertainty. A simple example of this is given by the fact that, for  $eeu\bar{u}$ , the difference in using constituent or current quark masses already amounts to 14%.

The cross-sections obtained with the above phase space coverage at a typical LEP2 energy,  $\sqrt{s} = 199.5$  GeV, are given in appendix B together with a detailed description of the standard input parameter set used.

## 7 Matrix elements for reweighting

It is common practice to define cross-sections for 4- $f$  processes considering only subsets of Feynman diagrams: CC03, NC02,  $t$ -channel single  $W$ . Although unphysical, as all the diagrams take part in the event probability, these definitions reflect the dominant component in the phase space region under study. Thus correction factors have to be evaluated to extract the relevant part of the experimentally measured cross-section. It is therefore useful to compute, for each event, the squared matrix elements  $|\mathcal{M}|^2$  corresponding to several potentially interesting subsets of Feynman diagrams. They can be used to determine their respective components in the unweighted sample. Moreover, calculating for each subset the matrix elements with the remaining graphs allows the interference between the two to be evaluated, thus completing the information.

The squared matrix elements corresponding to the following subsets are given in the standard DELPHI output:

1. CC03 (i.e.  $WW$ ),
2.  $t$ -channel component,
3. NC02 (i.e.  $ZZ$ ),
4.  $Z\gamma^*$ ,
5.  $\gamma^*\gamma^*$ ,
6. NC08 (i.e.  $ZZ + Z\gamma^* + \gamma^*\gamma^*$ ),
7. multiperipheral (neutral currents only),
8. multiperipheral  $\gamma\gamma$  only,
9.  $t$ -channel non-multiperipheral component.

In CC03-related analyses it is interesting to know the behaviour of the squared matrix element as a function of several physical input parameters:  $W$  mass,  $W$  width, trilinear gauge coupling (TGC) parameters. The  $W$  width in the Standard Model is not an independent parameter, but is defined by the  $W$  mass and couplings. Nevertheless, in the experimental fits, it can be useful to treat it as a free parameter: in WPHACT this possibility is provided, keeping the  $W$  mass and the couplings at their Standard Model values.

A compact and precise way of describing the functional dependence of the squared matrix element on the  $W$  mass and width is adopted. A suitable number of coefficients of the Chebyshev polynomial expansion of  $\log_{10} |\mathcal{M}|^2$  is computed in the physically interesting interval:  $[78.5, 82.5]$  GeV/ $c^2$  for the mass, and  $[0.2, 6.2]$  GeV/ $c^2$  for the width.

The functional dependence of the squared matrix element on the TGCs (the parametrization  $\Delta g_1^Z, \Delta\kappa_\gamma, \lambda_\gamma$  in [29] is used) is also given as part of the standard output. Since the cross-section is a quadratic function in term of these TGC parameters, the coefficients of this quadratic parametrization are computed by solving a linear system of equations obtained by evaluating the cross-section for a suitable number of combinations of TGC values (*e.g.* 10 coefficients to describe the variation of 3 parameters).



## 8 Summary

We have described the setup for 4- $f$  event generation chosen by the DELPHI collaboration for LEP2 measurements. The main difficulty in its construction consisted in interfacing in the optimal way the best features which were available at the end of the LEP2 generator workshop for the various 4- $f$  processes, in order to describe every corner of the phase space as accurately as possible. This is very important for physics measurements, with particular attention to the  $W$  sector, but also for the best evaluation of backgrounds to search processes.

## 9 Acknowledgements

We are grateful to S. Jadach, W. Placzek, M. Skrzypek, B. F. L. Ward and Z. Was for useful discussions and for the code used to implement the YFS exponentiated ISR in the DELPHI version of `WPHACT`. We thank M. Boonekamp and S. Todorova for discussions and collaboration on the phase space cuts and  $\gamma\gamma$  matching definition, E. Accomando and E. Maina for their collaboration and advice, and R. Sekulin for his careful reading and his comments on the manuscript.

## A Appendix: phase space cuts for 4- $f$ - $\gamma\gamma$ matching

The “4- $f$  like” region is defined as:

- $eeff$  where  $f \neq e$  double tag, i.e. both electron and positron have polar angle<sup>2</sup> of  $\theta_e > 10^\circ$ ;
- $eeff$  where  $f \neq e$  single tag, where the visible electron has a polar angle of  $\theta_e > 10^\circ$  and  $m(ff) > 40 \text{ GeV}/c^2$ ;
- $eeee$  with 3 or 4 visible electrons, i.e. with a polar angle of  $\theta_e > 10^\circ$ .

The “ $\gamma\gamma$  like” region is defined as:

- $eeqq$  single tag, where the visible electron has a polar angle of  $\theta_e > 10^\circ$  and  $3 < m(qq) < 40 \text{ GeV}/c^2$ ;
- $ee\mu\mu$  single tag, where the visible electron has a polar angle of  $\theta_e > 10^\circ$ ,  $m(\mu\mu) < 40 \text{ GeV}/c^2$  and at least one muon has  $\theta_\mu > 2^\circ$ ;
- $ee\tau\tau$  single tag, where the visible electron has a polar angle of  $\theta_e > 10^\circ$ ,  $m(\tau\tau) < 40 \text{ GeV}/c^2$  and at least one tau has  $\theta_\tau > 2^\circ$ ;
- $eeff$  where  $f \neq e$  double tag, i.e. both electron and positron have polar angle of  $2^\circ < \theta_e < 10^\circ$ ;
- $eeff$  where  $f \neq e$  single tag, i.e. the visible electron has a polar angle of  $2^\circ < \theta_e < 10^\circ$  and  $m(ff) > 40 \text{ GeV}/c^2$ ;
- $eeff$  where  $f \neq e$  no tag, with both electron and positron with a polar angle of  $\theta_e < 2^\circ$  and  $m(ff) > 40 \text{ GeV}/c^2$ ;
- $eeee$  quadruple tag, where the tagged electrons have a polar angle of  $\theta_e > 2^\circ$  but not all of them have  $\theta_e > 10^\circ$ ;
- $eeee$  triple tag, where the tagged electrons have  $\theta_e > 2^\circ$  but not all of them have  $\theta_e > 10^\circ$ , and the minimum of the invariant masses  $m(e^+e^-)$  is above  $40 \text{ GeV}/c^2$ ;
- $eeee$  double tag, where the tagged electrons have  $\theta_e > 2^\circ$  and the minimum of the invariant masses  $m(e^+e^-)$  is above  $40 \text{ GeV}/c^2$ .

The pure  $\gamma\gamma$  region is the one complementary to the two regions defined above.

---

<sup>2</sup>Here and below, equivalent conditions are implied on the supplements of the quoted values of the polar angle, i.e.  $\theta > x \Rightarrow \theta < 180^\circ - x$  and  $\theta < x \Rightarrow \theta > 180^\circ - x$ .

## B Appendix: Input parameter set

For the standard event generation the following input parameters have been used:

$$\begin{aligned}
 G_\mu &= 1.16639 \times 10^{-5} \text{ GeV}^{-2} \\
 M_W &= 80.4 \text{ GeV}/c^2 \\
 M_Z &= 91.187 \text{ GeV}/c^2 \\
 m_t &= 175 \text{ GeV}/c^2 \\
 M_H &= 115 \text{ GeV}/c^2 \text{ }^3 \\
 \alpha(Q^2 = 0) &= 1/137.0359895
 \end{aligned}$$

The  $G_\mu$  renormalization scheme is used, the running of  $\alpha$  is used in the low invariant mass regions and the running width is used for the boson propagators. The lepton masses are fixed at their PDG values [30]. The naive QCD correction is used for the boson width correction.

As an example of the results obtained with the above parameters and the phase space cuts discussed in the text, the cross-sections for all the processes at  $\sqrt{s} = 199.5 \text{ GeV}$  are listed in tables 3, 4 and 5. The total generated cross-section is  $82.95 \pm 0.03 \text{ pb}$ , where the error is purely statistical, corresponding to the accuracy of the integration.

---

<sup>3</sup>Used only in the DPA calculation; at Born level no diagram with Higgs boson exchange is considered.

| CC           |                                       |                    |   |                    |
|--------------|---------------------------------------|--------------------|---|--------------------|
| process type | final state                           | cross-section (pb) | final state                             | cross-section (pb) |
| CC09         | $\mu^- \bar{\nu}_\mu \nu_\tau \tau^+$ | 0.40756(9)         |   |                    |
| CC18         | $e^- \bar{\nu}_e \nu_\mu \mu^+$       | 0.50649(9)         | $e^- \bar{\nu}_e \nu_\tau \tau^+$       | 0.50333(9)         |
| CC10         | $\mu^- \bar{\nu}_\mu u \bar{d}$       | 1.2096(3)          | $\tau^- \bar{\nu}_\tau u \bar{d}$       | 1.2087(3)          |
|              | $\mu^- \bar{\nu}_\mu c \bar{s}$       | 1.2077(3)          | $\tau^- \bar{\nu}_\tau c \bar{s}$       | 1.2058(3)          |
|              | $\mu^- \bar{\nu}_\mu u \bar{s}$       | 0.06282(1)         | $\tau^- \bar{\nu}_\tau u \bar{s}$       | 0.06276(1)         |
|              | $\mu^- \bar{\nu}_\mu c \bar{d}$       | 0.06274(1)         | $\tau^- \bar{\nu}_\tau c \bar{d}$       | 0.06261(1)         |
|              | $\mu^- \bar{\nu}_\mu c \bar{b}$       | 0.0020876(5)       | $\tau^- \bar{\nu}_\tau c \bar{b}$       | 0.0020860(5)       |
| CC20         | $e^- \bar{\nu}_e u \bar{d}$           | 1.5300(3)          | $e^- \bar{\nu}_e c \bar{d}$             | 0.07786(1)         |
|              | $e^- \bar{\nu}_e c \bar{s}$           | 1.4981(3)          | $e^- \bar{\nu}_e c \bar{b}$             | 0.0025850(6)       |
|              | $e^- \bar{\nu}_e u \bar{s}$           | 0.07936(1)         |   |                    |
| CC11         | $s \bar{c} u \bar{d}$                 | 3.5744(7)          | $d \bar{c} c \bar{b}$                   | 0.00032050(7)      |
|              | $s \bar{c} u \bar{s}$                 | 0.18562(5)         | $b \bar{c} u \bar{d}$                   | 0.006187(1)        |
|              | $s \bar{c} c \bar{d}$                 | 0.18522(5)         | $b \bar{c} u \bar{s}$                   | 0.00032124(7)      |
|              | $s \bar{c} c \bar{b}$                 | 0.006172(1)        | $s \bar{u} u \bar{s}$ **                | 0.004831(1)        |
|              | $d \bar{u} u \bar{s}$                 | 0.18606(5)         | $d \bar{c} c \bar{d}$ **                | 0.004809(1)        |
|              | $d \bar{c} u \bar{d}$                 | 0.18558(5)         | $b \bar{c} c \bar{b}$ **                | 0.000005337(2)     |
|              | $d \bar{c} u \bar{s}$                 | 0.009638(1)        |   |                    |
| Mixed        |                                       |                    |   |                    |
| process type | final state                           | cross-section (pb) | final state                             | cross-section (pb) |
| MIX19        | $\mu^- \mu^+ \nu_\mu \bar{\nu}_\mu$   | 0.22697(4)         | $\tau^- \tau^+ \nu_\tau \bar{\nu}_\tau$ | 0.21412(4)         |
| MIX56        | $e^- e^+ \nu_e \bar{\nu}_e$           | 0.4197(1)          |   |                    |
| MIX43        | $d \bar{d} u \bar{u}$                 | 1.9070(3)          | $s \bar{s} c \bar{c}$                   | 1.8582(3)          |

Table 3: Cross-sections for all the charged and mixed current 4- $f$  processes at  $\sqrt{s} = 199.5$  GeV with the phase space cuts discussed in the text. For CC processes the charge conjugate final state is also included. Those labelled with \*\* are only the CC contribution to the full process; the neutral current part is given in the NC table. The errors quoted are purely statistical, corresponding to the accuracy of the integration.

| NC (not $\gamma\gamma$ compatible) |   |                    |   |                    |
|------------------------------------|---|--------------------|---|--------------------|
| process type                       | final state                                     | cross-section (pb) | final state                                       | cross-section (pb) |
| NC06                               | $\nu_\mu \bar{\nu}_\mu \nu_\tau \bar{\nu}_\tau$ | 0.008784(2)        |   |                    |
| NC12                               | $\nu_\mu \bar{\nu}_\mu \nu_e \bar{\nu}_e$       | 0.009374(3)        | $\nu_\tau \bar{\nu}_\tau \nu_e \bar{\nu}_e$       | 0.009378(3)        |
| NC12                               | $\nu_\mu \bar{\nu}_\mu \nu_\mu \bar{\nu}_\mu$   | 0.004358(1)        | $\nu_\tau \bar{\nu}_\tau \nu_\tau \bar{\nu}_\tau$ | 0.004358(1)        |
| NC36                               | $\nu_e \bar{\nu}_e \nu_e \bar{\nu}_e$           | 0.004845(2)        |   |                    |
| NC10                               | $u \bar{u} \nu_\mu \bar{\nu}_\mu$               | 0.04149(3)         | $c \bar{c} \nu_\mu \bar{\nu}_\mu$                 | 0.02611(1)         |
|                                    | $u \bar{u} \nu_\tau \bar{\nu}_\tau$             | 0.04149(3)         | $c \bar{c} \nu_\tau \bar{\nu}_\tau$               | 0.02611(1)         |
| NC19                               | $u \bar{u} \nu_e \bar{\nu}_e$                   | 0.06211(4)         | $c \bar{c} \nu_e \bar{\nu}_e$                     | 0.03291(1)         |
| NC64                               | $u \bar{u} u \bar{u}$                           | 0.0776(1)          | $c \bar{c} c \bar{c}$                             | 0.03741(1)         |
| NC32                               | $u \bar{u} c \bar{c}$                           | 0.11257(8)         |   |                    |
| NC10                               | $\mu^- \mu^+ \nu_\tau \bar{\nu}_\tau$           | 0.022940(9)        | $\tau^- \tau^+ \nu_\mu \bar{\nu}_\mu$             | 0.010351(2)        |
| NC20                               | $e^- e^+ \nu_\mu \bar{\nu}_\mu$                 | 0.11120(6)         | $e^- e^+ \nu_\tau \bar{\nu}_\tau$                 | 0.11120(6)         |
| NC19                               | $\mu^- \mu^+ \nu_e \bar{\nu}_e$                 | 0.03811(2)         | $\tau^- \tau^+ \nu_e \bar{\nu}_e$                 | 0.013485(4)        |
| NC24                               | $\mu^- \mu^+ u \bar{u}$                         | 0.0775(2)          | $\tau^- \tau^+ u \bar{u}$                         | 0.04264(3)         |
|                                    | $\mu^- \mu^+ c \bar{c}$                         | 0.06007(5)         | $\tau^- \tau^+ c \bar{c}$                         | 0.02891(1)         |
| NC19                               | $d \bar{d} \nu_e \bar{\nu}_e$                   | 0.03291(3)         | $b \bar{b} \nu_e \bar{\nu}_e$                     | 0.03058(2)         |
|                                    | $s \bar{s} \nu_e \bar{\nu}_e$                   | 0.022758(9)        |   |                    |
| NC10                               | $d \bar{d} \nu_\mu \bar{\nu}_\mu$               | 0.02672(2)         | $d \bar{d} \nu_\tau \bar{\nu}_\tau$               | 0.02672(2)         |
|                                    | $s \bar{s} \nu_\mu \bar{\nu}_\mu$               | 0.02550(1)         | $s \bar{s} \nu_\tau \bar{\nu}_\tau$               | 0.02550(1)         |
|                                    | $b \bar{b} \nu_\mu \bar{\nu}_\mu$               | 0.021165(7)        | $b \bar{b} \nu_\tau \bar{\nu}_\tau$               | 0.021165(7)        |
| NC32                               | $s \bar{s} u \bar{u}$                           | 0.11221(8)         | $b \bar{b} u \bar{u}$                             | 0.09950(4)         |
|                                    | $d \bar{d} c \bar{c}$                           | 0.07664(4)         | $b \bar{b} c \bar{c}$                             | 0.06284(2)         |
| NC24                               | $\mu^- \mu^+ \tau^- \tau^+$                     | 0.02219(3)         |   |                    |
| NC48                               | $\mu^- \mu^+ \mu^- \mu^+$                       | 0.01842(6)         | $\tau^- \tau^+ \tau^- \tau^+$                     | 0.005381(2)        |
| NC64                               | $d \bar{d} d \bar{d}$                           | 0.03913(2)         | $b \bar{b} b \bar{b}$                             | 0.025382(5)        |
|                                    | $s \bar{s} s \bar{s}$                           | 0.03608(1)         |   |                    |
| NC24                               | $\mu^- \mu^+ d \bar{d}$                         | 0.06194(6)         | $\tau^- \tau^+ d \bar{d}$                         | 0.02987(1)         |
|                                    | $\mu^- \mu^+ s \bar{s}$                         | 0.06065(5)         | $\tau^- \tau^+ s \bar{s}$                         | 0.02880(1)         |
|                                    | $\mu^- \mu^+ b \bar{b}$                         | 0.05516(2)         | $\tau^- \tau^+ b \bar{b}$                         | 0.024889(5)        |
| NC32                               | $d \bar{d} s \bar{s}$                           | 0.07531(3)         | $s \bar{s} b \bar{b}$                             | 0.06128(2)         |
|                                    | $d \bar{d} b \bar{b}$                           | 0.06413(2)         |   |                    |

Table 4: Cross-sections for all the neutral current 4- $f$  processes not compatible with  $\gamma\gamma$ -like final states at  $\sqrt{s} = 199.5$  GeV with the phase space cuts discussed in the text. The errors quoted are purely statistical, corresponding to the accuracy of the integration.

| NC ( $\gamma\gamma$ compatible) |                         |                                  |  |
|---------------------------------|-------------------------|----------------------------------|--|
| process type                    | final state             | 4- $f$ region cross-section (pb) | $\gamma\gamma$ region cross-section (pb) |
| NC144                           | $e^- e^+ e^- e^+$       | 2.687(9)                         | 5.225(6)                                 |
| NC48                            | $e^- e^+ \mu^- \mu^+$   | 1.093(2)                         | 21.19(2)                                 |
|                                 | $e^- e^+ \tau^- \tau^+$ | 0.5340(6)                        | 7.385(2)                                 |
| NC48                            | $e^- e^+ u \bar{u}$     | 1.171(2)                         | 10.382(4)                                |
|                                 | $e^- e^+ c \bar{c}$     | 0.5761(6)                        | 7.378(2)                                 |
| NC48                            | $e^- e^+ d \bar{d}$     | 0.3682(6)                        | 1.6599(8)                                |
|                                 | $e^- e^+ s \bar{s}$     | 0.3327(6)                        | 1.4825(5)                                |
|                                 | $e^- e^+ b \bar{b}$     | 0.24304(8)                       | 0.36173(9)                               |

Table 5: Cross-sections for the neutral current 4- $f$  processes with  $\gamma\gamma$ -compatible final states, i.e.  $eell$  and  $eeqq$  where  $l$  is a charged lepton and  $q$  a quark, at  $\sqrt{s} = 199.5$  GeV. The cross-section is shown separately for the two different phase space regions described in appendix A. The errors quoted are purely statistical, corresponding to the accuracy of the integration.

## References

- [1] Physics at LEP2, G. Altarelli, T. Sjöstrand and F. Zwirner eds., CERN 96-01 (1996).
- [2] D. Bardin *et al.*, *Event Generators for WW Physics*, in Ref. [1], vol.2 p.3 [hep-ph/9709270].
- [3] F. Boudjema *et al.*, *Standard Model Processes at LEP2*, in Ref. [1], vol.1 p.207 [hep-ph/9601224].
- [4] M. Grünewald *et al.*, *Four-Fermion Production in Electron-Positron Collisions*, in *Report of the Working Groups on precision calculations for LEP2 physics*, S. Jadach, G. Passarino and R. Pittau eds., CERN 2000-009 (2000) 1 [hep-ph/0005309].
- [5] W. Beenakker, F.A. Berends and A.P. Chapovsky, Nucl. Phys. **B548** (1999) 3.
- [6] A. Denner, Fortschr. Phys. **41** (1993) 307;  
A. Denner, S. Dittmaier and G. Weiglein, Nucl. Phys. **B440** (1995) 95;  
A. Denner, S. Dittmaier and M. Roth, Nucl. Phys. **B519** (1998) 39.
- [7] A. Denner, S. Dittmaier, M. Roth and D. Wackerth, Nucl. Phys. **B560** (1999) 33;  
A. Denner, S. Dittmaier, M. Roth and D. Wackerth, Nucl. Phys. **B587** (2000) 67.
- [8] S. Jadach, W. Placzek, M. Skrzypek, B. F. L. Ward and Z. Was, Phys. Lett. **B417** (1998) 326;  
S. Jadach, W. Placzek, M. Skrzypek, B. F. L. Ward and Z. Was, Comp. Phys. Commun. **140** (2001) 432.
- [9] J. Fleischer, F. Jegerlehner and M. Zralek, Z. Phys. **C42** (1989) 409.
- [10] A.P. Chapovsky and V.A. Khoze, Eur. Phys. J. **C9** (1999) 449.
- [11] R. Chierici and F. Cossutti, Eur. Phys. J. **C23** (2002) 65.
- [12] S. Jadach, W. Placzek, M. Skrzypek, B. F. L. Ward and Z. Was, Comp. Phys. Commun. **140** (2001) 475.
- [13] S. Jadach, W. Placzek, M. Skrzypek, B. F. L. Ward and Z. Was, Comp. Phys. Commun. **119** (1999) 272.
- [14] E. Accomando and A. Ballestrero, Comp. Phys. Commun. **99** (1997) 270;  
E. Accomando, A. Ballestrero and E. Maina, hep-ph/0204052 (2002), to be published in Comp. Phys. Commun.
- [15] M. Boonekamp, DAPNIA-SPP-01-16 (2001) [hep-ph/0111213].
- [16] Y. Kurihara, J. Fujimoto, T. Muneisha and Y. Shimizu, Progress of Theoretical Physics **96** (1996) 1223.
- [17] E. Accomando, A. Ballestrero and E. Maina, Phys. Lett. **B479** (2000) 209.
- [18] T. Sjöstrand *et al.*, Comp. Phys. Commun. **135** (2001) 238.
- [19] E. Barberio and Z. Was, Comp. Phys. Commun. **79** (1994) 291.
- [20] S. Jadach, Z. Was, R. Decker and J.H. Kuehn, Comp. Phys. Commun. **76** (1993) 361.
- [21] L. Lönnblad, Comp. Phys. Commun. **71** (1992) 15.
- [22] G. Corcella *et al.*, JHEP **01** (2001) 10 [hep-ph/0011363].
- [23] I.G. Knowles *et al.*, *QCD Event Generators*, in Ref. [1], vol.2 p.103 [hep-ph/9601212].
- [24] DELPHI Collaboration, P. Abreu *et al.*, Zeit. Phys. **C73** (1996) 11.
- [25] S. Jadach, B. F. L. Ward and Z. Was, Comp. Phys. Commun. **130** (2000) 260.
- [26] M.L. Mangano *et al.*, *Event Generators for Discovery Physics*, in Ref. [1], vol.2 p.309 [hep-ph/9602203].
- [27] F.A. Berends, P.H. Daverveldt and R. Kleiss, Comp. Phys. Commun. **40** (1986) 271.
- [28] F.A. Berends, P.H. Daverveldt and R. Kleiss, Comp. Phys. Commun. **40** (1986) 285.
- [29] G. Gounaris *et al.*, *Triple Gauge Boson Couplings*, in Ref. [1], vol.1 p.525 [hep-ph/9601233].

[30] The Particle Data Group, D. E. Groom *et al.*, Eur. Phys. J. **C15** (2000) 1.